Desalination and Water Treatment
www.deswater.com

doi: 10.5004/dwt.2018.21657

104 (2018) 45–50
February

Fouling due to $CaSO_4$ scale formation in forward osmosis (FO), reverse osmosis (RO), and pressure assisted forward osmosis (PAFO)

Hwan Kim[a], Sengmin Park[a,b], Yongjun Choi[b], Sangho Lee[b,*], Juneseok Choi[c]

[a]*Korea Testing Laboratory, Chungghi-ro, Jinju-si, Geyongsangnam-do, 52852, Korea*
[b]*School of Civil and Environmental Engineering, Kookmin University, Jeongneung-Dong, Seongbuk-Gu, Seoul, 136-702, Korea, Tel. 82 2 910 4529; Fax: 82 2 910 4939; email: sanghlee@kookmin.ac.kr*
[c]*Korea Institute of Construction Technology, 1190, Simindae-Ro, Ilsanseo-Gu, Goyang-Si, Gyeonggi-Do, Korea*

Received 27 August 2017; Accepted 28 October 2017

ABSTRACT

Forward osmosis (FO) is a water treatment technique that utilizes a semi-permeable membrane to remove dissolved solutes from water by the use of a salinity gradient. Unlike reverse osmosis (RO), the driving force of FO is not the hydraulic pressure and thus FO does not need high energy to pressurize feed water. However, the efficiency of FO may be deteriorated by the occurrence of fouling induced by the precipitation of inorganic scales if the feed water includes salts such as $CaCO_3$, $CaSO_4$, or silica. The focus of this study was the investigation of FO membrane fouling caused by $CaSO_4$ scale formation. The changes in flux, saturation degree, and the turbidity of the brine were measured as a function of operation time in a laboratory scale FO system. The fouling characteristics of FO were compared with those of RO and pressure-assisted FO (PAFO) under similar filtration conditions. A theoretical model considering different scale formation mechanisms was also applied to quantitatively analyze FO fouling.

Keywords: Forward osmosis; Reverse osmosis; Pressure-retarded osmosis; Scale formation; Fouling

1. Introduction

As available water resources are depleting, seawater desalination has become a technically and economically feasible option for ongoing water supply [1,2]. In arid areas where there is insufficient fresh water, seawater desalination is an inevitable choice. In addition, climate change has increased the risk of prolonged drought in many other regions [3], making desalination increasingly attractive. Current desalination systems are classified as either thermal or reverse osmosis (RO) technologies [4]. Thermal technologies use heat to vaporize water to remove salts while RO technology uses hydraulic pressure to overcome osmotic pressure of the seawater to produce fresh water. Although they are widely used, their high energy consumption is one of the critical issues to be addressed prior to further widespread application of desalination technologies [5].

As an alternative option, forward osmosis (FO) has been actively investigated as a novel desalination technique [6]. FO exploits the osmotic pressure difference between the feed (low solute concentration) and the draw (high solute concentration) to induce water flows through an osmotic membrane [7]. FO itself does not need high pressure for its operation [8]. Depending on draw solute recovery methods, however, high pressure may be needed in FO systems to separate fresh water from draw solution [9]. Nevertheless, FO still holds potential as a low energy desalination technique. Moreover, FO is being considered for wastewater treatment and reuse [10]. Of course, there are several issues to be addressed

* Corresponding author.

before FO is widely accepted by industry and one of them is the control of membrane fouling [6,11].

Among various fouling phenomenon, scale formation is a common problem in seawater and brackish water desalination. Scale formation can occur when sparingly soluble salts, which are present in the natural water, are concentrated beyond their solubility limit in the feed stream. Since the salts such as $CaCO_3$, $CaSO_4$, and silica crystallize and grow on the surface of membranes, the product flow through the membrane decrease gradually [12,13]. Scale formation may be even more serious in FO process than RO process if FO is applied to treat water with high salt concentrations or at high recovery conditions [11].

Although scale formation has been widely investigated in RO processes, there are still unfulfilled information needs for better understanding of this problem. Two different scale formation mechanisms have been reported in RO processes, which include surface (heterogeneous) crystallization and bulk (homogeneous) crystallization. There are also a lot of factors affecting the scale formation and subsequent RO fouling, such as solution pH [14], temperature [15], and the presence of dissolved organics [16,17]. Scale formation can be mitigated with the use of antiscalant, change of operating conditions, and application of pretreatment to lower the scaling potential of feed water [18]. However, relatively few works have been done for FO scale formation [19]. Moreover, there is no reliable model available to predict FO fouling resulted from inorganic scaling.

The objective of this paper was to elucidate the mechanisms of fouling due to scale formation in FO process. A theoretical model combining solution-diffusion model and crystallization theory was devised to predict the scale formation of FO membrane system. This model was intended to provide insight into the control of scale formation problems in FO process. In addition to FO, scale formation in RO and PAFO was also investigated and compared. The novelty of this study lies in its development of a model to analyze scale formation in FO, RO, PAFO systems.

2. Model development

A model for FO process was derived based on membrane transport equations and modified by the crystallization theory to analyze the scale formation effect. The model was applied to obtain the fouling factors by fitting the experimental results.

2.1. Modified solution-diffusion model for FO process

For an osmotic membrane process, the water flux is described as [20]:

$$J_w = L_v\left(\Delta P + \pi_{D,b}\exp\left(-\frac{J_w}{k_D}\right) - \pi_{F,b}\exp\left(\frac{J_w}{k_F}\right)\right) \quad (1)$$

where J_w is the water flux through the FO membrane, L_v is the water permeability constant, ΔP is the imposed hydraulic pressure, $\pi_{D,b}$ is the osmotic pressure of the draw solution, $\pi_{F,b}$ is the osmotic pressure of the feed solution, k_D is the internal mass transfer coefficient, and k_F is the external mass transfer coefficient for external concentration polarization. It is an FO system at $\Delta P = 0$ and $\pi_{D,b} \neq 0$ while it is an RO system at $\Delta P \neq 0$ and $\pi_{D,b} = 0$. If $\Delta P \neq 0$ and $\pi_{D,b} \neq 0$, it is a PAFO system.

The external and internal mass transfer coefficients, k_F and k_D, are presented as [21,22]:

$$k_F = 1.62\,\mathrm{Re}^{1/3}\,\mathrm{Sc}^{1/3}\left(\frac{D}{d_h}\right)\left(\frac{d_h}{L}\right)^{1/3} \quad (2)$$

$$k_D = \frac{D\varepsilon}{\tau l} \quad (3)$$

where Re is the Reynolds number, Sc is the Schmidt number, D is the diffusion coefficient, d_h is the hydraulic diameter of the membrane feed channel, L is the length of the feed channel, ε is the FO membrane support porosity, l is the support thickness, and τ is the support tortuosity.

On the other hand, J_s and C_p can be calculated using solution-diffusion model as follows:

$$J_s = J_w c_p = L_s\left(c_b\exp\left(\frac{J_w}{k_F}\right) - c_p\right) \quad (4)$$

2.2. Models for scale formation

It has been reported that there are two different scale formation mechanisms including bulk crystallization and surface crystallization. In case of the bulk crystallization, fouling occurs by the cake layer made of inorganic crystal particles. In case of the surface crystallization, fouling occurs through the surface blockage mechanisms. Accordingly, the water flux equation was derived from Eq. (1) by including the two mechanisms:

$$J_w = \frac{\Delta P + \pi_{D,b}\exp\left(-\frac{J_w}{k_D}\right) - \pi_{F,b}\exp\left(\frac{J_w}{k_F}\right)}{\eta\left(R_m + R_c\right)} \times \frac{A - A_b}{A} \quad (5)$$

where η is the viscosity of the permeate; R_m is the intrinsic resistance of the membrane; R_c is the cake layer resistance; A is the area of the membrane; and A_b is the area occupied by surface crystals on the membrane surface. Assuming that the thickness of surface crystal is almost constant [23], the A_b is given by:

$$A_b = \beta m_s \quad (6)$$

where β is the coefficient for surface crystals and m_s is the weight of surface crystals. On the other hand, the cake resistance R_c is obtained from the Darcy's law:

$$R_c = \frac{\alpha m_c}{A} \quad (7)$$

where α is the specific cake resistance and m_c is the cake mass.

According to the crystallization theory, the growth rate of surface crystals is given by:

$$\frac{dm_s}{dt} = k_s A\left(c_w - c_s\right)^n \quad (8)$$

where k_s is the rate constant of surface crystallization; c_w is the wall concentration; c_s is the saturation concentration; and n is the order of reaction rate.

On the other hand, the rate of bulk crystallization is written as:

$$\frac{dm_c}{dt} = k_c s_p \psi \left(c_b - c_s\right)^m = k_b \left(c_b - c_s\right)^m \quad (9)$$

where k_c is the rate constant of bulk crystallization; s_p is the active surface area on bulk crystals; c_b is the bulk concentration; ψ is the deposition probability of crystal particles; m is the order of reaction rate; and k_b is the apparent rate constant of bulk crystallization ($=k_c s_p \psi$).

2.3. Mass balance equation

In batch filtration, permeate flux and concentrations changes with time due to the continuous removal of the permeate volume (V_p) from the system. In this case, the volume concentration factor (VCF), which is defined as the ratio of the initial feed volume (V_i) to concentrate volume (V_c), indicates the extent of concentration:

$$\mathrm{VCF} = \frac{V_f}{V_c} = \frac{V_f}{V_f - V_c} \quad (10)$$

Based on the mass balance, c_b is given by:

$$c_b(t) = \frac{\mathrm{VCF}(t) c_f}{\mathrm{VCF}(t)(1-R)+R} - \frac{\mathrm{VCF}(t)}{V_f}\left(m_s(t) + m_c(t)\right) \quad (11)$$

By simultaneously solving Eqs. (1)–(11) for a given geometry, the flux and solute concentrations can be calculated as functions of time and VCF. The equations are solved using the explicit Euler method. L_v and L_s were obtained from stirred cell experiments. The fouling factors including α, β, k_s, and k_b were determined by fitting the model calculation to experimental data.

3. Experimental

3.1. Feed water and membrane

Saturated $CaSO_4$ solution was used as the feed solution, which was prepared by dissolving 2,090 mg/L of $CaSO_4$ into DI water and then filtered using a glass microfiber filter (Whatman, Grade GF/C, USA). An ion chromatography (DIONEX, USA) was used to measure the concentrations of $CaSO_4$ in the feed. In addition, an electronic conductivity meter (Orion, USA) was also used. A turbidimeter (DRT-100B, USA) was used to determine the turbidity of the brine. The membrane used for the experiment was HTI membrane (Lifepack, HTI, USA). The membrane was made of cellulose triacetate. The rejection of NaCl and $CaSO_4$ by this membrane was over 97%.

3.2. Experimental setup

Fig. 1 depicts the overall process diagram of the cross-flow FO equipment. A plate-and-frame FO membrane module, a temperature controller, two pumps, a feed tank, and a draw tank, were included in the FO equipment. The FO module was fabricated to have one feed flow channel and one draw flow channel. Each channel had dimensions of 12.4 cm length, 7.4 cm width, and 2 cm height. The effective membrane area was 92 cm^2. The flow rates were set to 0.7 L/min. Using the temperature controller, the feed temperature and draw solution temperature were set to 25°C. The water flux was monitored by an electronic balance with a communication port.

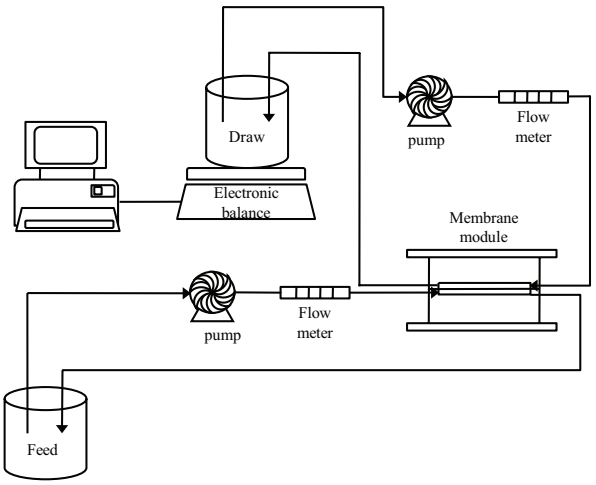

Fig. 1. Experimental setup for cross-flow FO experiments.

Experiments were performed for the examination of the progress of scale formation in FO mode. There were two types of system operation, including FO, RO, and PAFO modes. In FO mode, only the osmotic pressure difference is used to produce water flux. The draw solution was 4 M of NaCl, which lead to have osmotic driving force. On the other hand, only hydraulic pressure was applied in RO mode. In PAFO mode, both osmotic and hydraulic pressures were applied as the driving force. A 4 M NaCl solution was used as the draw solution and the hydraulic pressure was 5 bar.

The initial volume of feed solution was 1 L. Total dissolved solid and turbidity were determined using a conductivity meter.

4. Results and discussion

4.1. Scale formation in FO process

Fig. 2(a) shows the permeate flux of cross-flow FO filtration as a function of time. The feed solution was $CaSO_4$ saturated solution and the draw solution was 4 M NaCl solution. A permeate flux decline was observed only at the beginning, indicating the fouling through scale formation was not significant in FO system. Compared with the results of RO treatment of $CaSO_4$ solution in the literatures [24–26], it is likely that FO has lower fouling potential. This may be attributed to 1) the hydrophilic properties of the membrane that is inherently more resistance against fouling and 2) negligible hydraulic pressure applied in FO operation. In addition, the permeate flux is relatively low, leading to a low fouling propensity. After the operation of 650 min, the flux was reduced by 17 %.

Although the fouling was not significant, VCF continuously increased. As shown in Fig. 2(b), the VCF exponentially

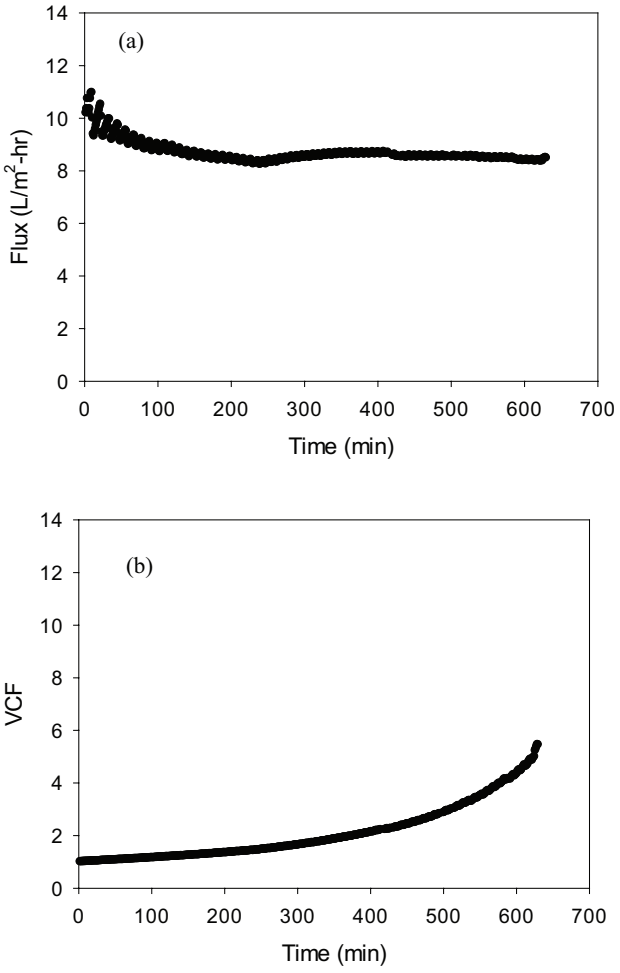

Fig. 2. Changes in flux and VCF with time for c_{Draw} = 4 M, ΔP = 0 kPa, Q_{conc} = 0.7 L/min. (a) Permeate flux, (b) VCF.

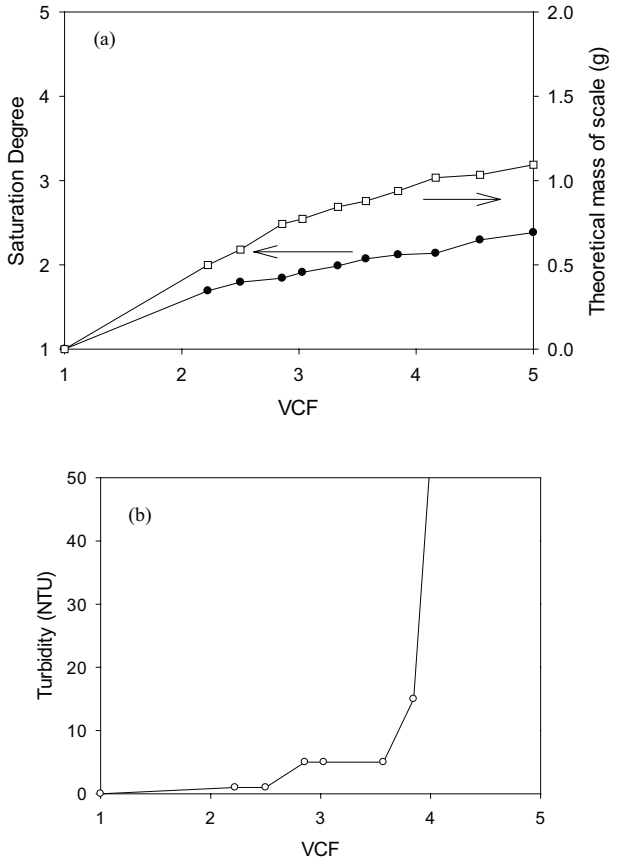

Fig. 3. Changes in saturation degree and turbidity with time for c_{Draw} = 4 M, ΔP = 0 kPa, Q_{conc} = 0.7 L/min. Symbols: saturation degree (●), theoretical mass of scale (□), and concentrate turbidity (○).

increased up to 6.0, implying that the feed solution was concentrated more than 5~6 times. As demonstrated in Fig. 2(a), flux decline after the operation time of 400 min was negligible even if the VCF exceeded 2.0. This suggests that FO fouling did not occur under the condition of high scale formation.

During the FO experiment, the saturation degree, which is expressed as the ratio of the $CaSO_4$ concentration in the brine to the initial $CaSO_4$ concentration (or the saturated concentration in this study), was measured. If there is no scale formation, the saturation degree is linearly proportional to the VCF. However, as depicted in Fig. 3(a), the saturation degree was always lower than the VCF, indication that the $CaSO_4$ crystallization occurred during the FO operation. Based on the mass balance analysis, the amount of scales formed during the FO operation was determined. In Fig. 3(a), the saturation degree was 2.3 at the final VCF of 5, which represents about 44% of total $CaSO_4$ was precipitated. More than 1.1 g of $CaSO_4$ was predicated at VCF of 5.0.

Fig. 3(b) shows the turbidity of the brine as a function of VCF. Above the VCF of 2.5, the turbidity of brine increased with increasing VCF. This is an evidence that the bulk crystallization of $CaSO_4$ occurred. With the progress of the bulk crystallization, the crystal particles are formed in the solution and recirculated together with the brine flow. On the other hand, the surface crystallization may not be as important as the bulk crystallization because a large amount of crystal particles were formed in the bulk phase.

4.2. Comparison of model fits with experimental results

The model developed in this study was applied to fit the experiments in Figs. 2(a) and 3(a). The results are shown in Fig. 3. It was assumed that only bulk crystallization occurs in FO systems [27] and thus fouling parameters such as k_c and α were determined. The k_F and k_D were calculated to be 2.246×10^{-6} m/s and 1.8×10^6 s/m, respectively. Although there are some differences, the model matches the trends of the experimental data well. It is evident from Fig. 4(a) that the flux decline is relatively small even with increasing filtration time, probably because of the small fouling potential of FO membrane. The model was also found to match the changes in the saturation degree with VCF. From the model fit, the k_b and α were calculated as 1.0×10^{-6} kg/s and 1.0×10^{15} m/kg, respectively.

The model parameters k_b and α represent the rate of bulk crystallization and the specific resistance of the foulant layer on the membrane surface. If k_b is high, the scale formation rapidly occurs, which determines the amount of crystals formed during the operation. However, if α is low,

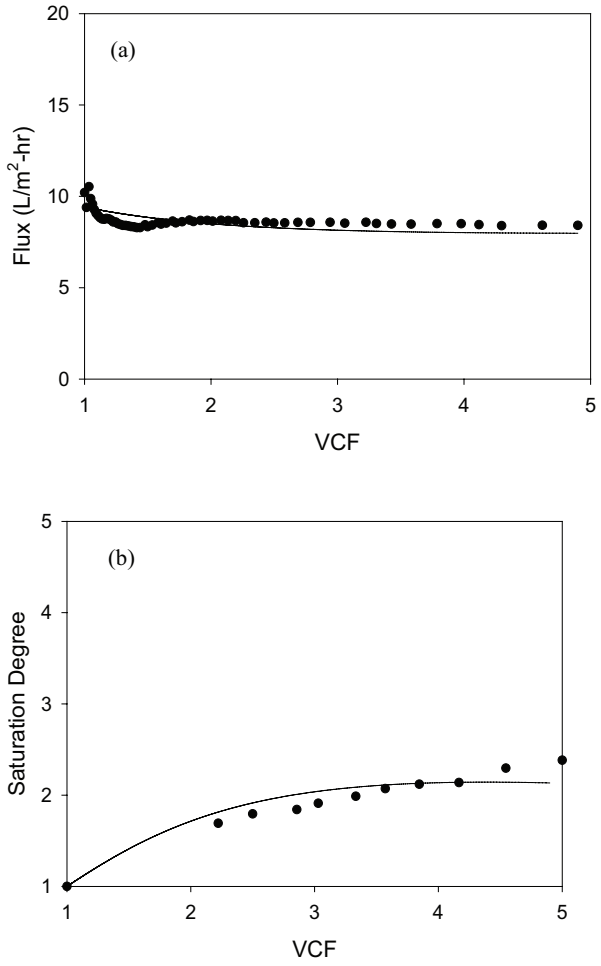

Fig. 4. Comparison of model calculations with experimental data. Experiments: •; model: —; conditions: c_{Draw} = 4 M; ΔP = 0 kPa, Q_{conc} = 0.7 L/min. (a) Permeate flux, (b) saturation degree and concentrate turbidity.

the foulant layer may not have enough hydraulic resistance to induce flux decline. In the case of FO, it seems that the flux decline is not serious due to the low α value.

4.3. Comparison of FO with RO and PAFO

Experiments were also carried out in RO and PAFO modes under similar conditions except for draw solution concentration and applied pressure. In Fig. 5, the results of the calculated flux by the model were compared with the experimentally determined flux for RO mode. The applied pressure was 1,000 kPa, leading to a higher flux than FO mode. The draw concentration was set to zero. Except for the data at initial stage of operation, the model reasonably matched the experimental results. In this case, the k_b and α were calculated as 1.0×10^{-5} kg/s and 2.0×10^{15} m/kg, respectively, which are much higher values than those in FO system. This suggests that the crystallization rate and specific cake resistance are higher in RO mode than in FO mode. The high α value in the RO mode can be explained by the hydraulic pressure applied to the foulant layer on the surface of the membrane. The α value seems to increase as a result of the compaction under high pressure.

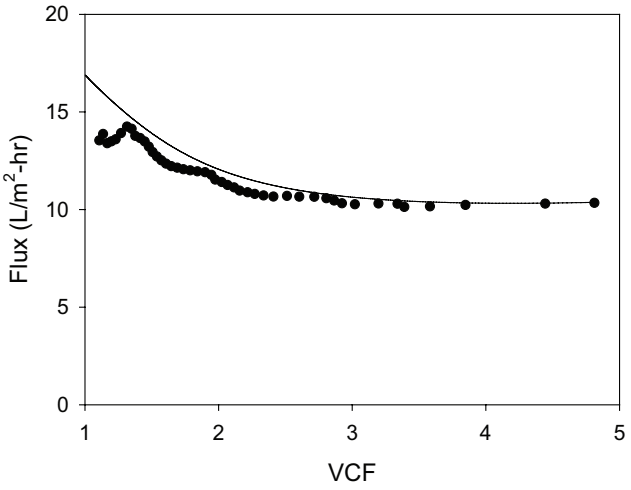

Fig. 5. Comparison of model calculations with experimental data in RO mode. Experiments: •; model : —; conditions: c_{Draw} = 0 M; ΔP = 1,000 kPa; Q_{conc} = 0.7 L/min.

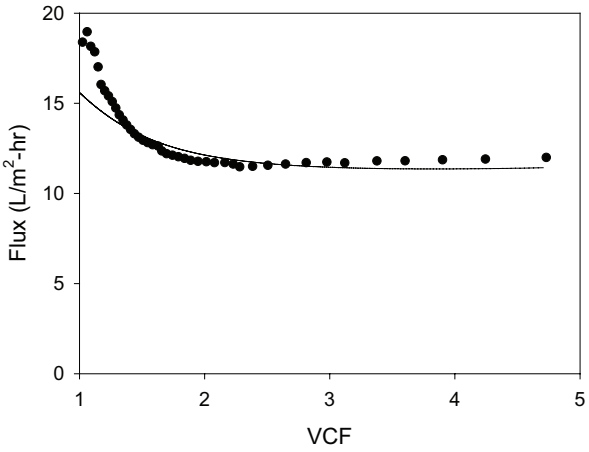

Fig. 6. Comparison of model calculations with experimental data in PAFO mode. Experiments: •; model: —; conditions: c_{Draw} = 4 M; ΔP = 500 kPa; Q_{conc} = 0.7 L/min.

Fig. 6 illustrates the experimental flux and model fit as a function of operation time in PAFO mode. The applied pressure was 500 kPa and the draw concentration was 4 M. Except for the initial conditions, the model matched the experiments well. The k_b and α for PAFO mode were calculated as 5.0×10^{-5} kg/s and 1.0×10^{15} m/kg, respectively. It is evident from the model calculations that the crystallization in PAFO mode is faster than in FO mode, indicating that the applied pressure affects the crystallization rate. This may be also attributed to the higher flux in PAFO than that in FO, which accelerates the crystallization.

4.4. Model validation

The model calculations for the permeate flux and experimental results are compared in Fig. 7. Although there were some deviations, the model has reasonable matches with the experimental data. The difference in the flux between the model fits and experimental data seems to increase at high

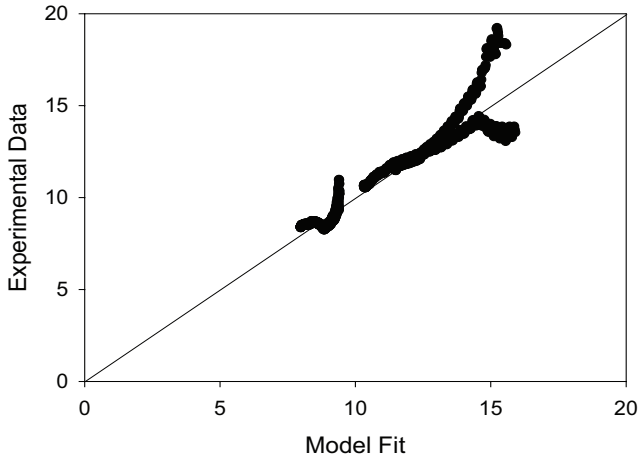

Fig. 7. Correlation between model calculations and experiments for FO, RO, and PAFO modes.

flux conditions. This is attributed to the deviations in the PAFO operation at low VCF condition. However, the model generally captures the overall trend of flux variations and the R^2 was estimated to 0.904.

5. Conclusion

In this work, FO fouling behaviors due to scale formation was experimentally investigated and compared with those in RO and PAFO systems. The following conclusions were drawn:

- The $CaSO_4$ scale formation on FO membrane was less severe than on RO membrane reported in the previous works. This is attributed to the hydrophilic characteristics of the FO membrane and lack of hydraulic pressure.
- A model combining modified solution-diffusion model with crystallization kinetics was developed and applied to analyze scale formation in FO, RO, and PAFO systems. The model fits the experiments well ($R^2 = 0.90$).
- Based on the model calculations, it is likely that the rate of $CaSO_4$ crystallization was accelerated by the applied pressure. The specific cake resistance was higher in RO mode than in FO and PAFO modes, suggesting that the compaction of cake layer may occur under high pressure conditions.

Acknowledgments

This research was supported by a grant (17IFIP-B065893-05) from Industrial Facilities & Infrastructure Research Program funded by Ministry of Land, Infrastructure and Transport of Korean government and also supported through the National Research Foundation of Korea (NRF) funded by the Ministry of Science and ICT (NRF-2017M1A2A2047551).

References

[1] M. Wilf, C. Bartels, Optimization of seawater RO systems design, Desalination, 173 (2005) 1–12.
[2] S.A. Avlonitis, K. Kouroumbas, N. Vlachakis, Energy consumption and membrane replacement cost for seawater RO desalination plants, Desalination, 157 (2003) 151–158.
[3] P. Tram Vo, H.H. Ngo, W. Guo, J.L. Zhou, P.D. Nguyen, A. Listowski, X.C. Wang, A mini-review on the impacts of climate change on wastewater reclamation and reuse, Sci. Total Environ., 494–495 (2014) 9–17.
[4] L.F. Greenlee, D.F. Lawler, B.D. Freeman, B. Marrot, P. Moulin, Reverse osmosis desalination: water sources, technology, and today's challenges, Water Res., 43 (2009) 2317–2348.
[5] N. Voutchkov, Energy use for membrane seawater desalination – current status and trends, Desalination, 431 (2018) 2–14.
[6] N. Akther, A. Sodiq, A. Giwa, S. Daer, H.A. Arafat, S.W. Hasan, Recent advancements in forward osmosis desalination: a review, Chem. Eng. J., 281 (2015) 502–522.
[7] M. Qasim, N.A. Darwish, S. Sarp, N. Hilal, Water desalination by forward (direct) osmosis phenomenon: a comprehensive review, Desalination, 374 (2015) 47–69.
[8] Y. Cai, X.M. Hu, A critical review on draw solutes development for forward osmosis, Desalination, 391 (2016) 16–29.
[9] D.J. Johnson, W.A. Suwaileh, A.W. Mohammed, N. Hilal, Osmotic's potential: an overview of draw solutes for forward osmosis, Desalination, 434 (2018) 100–120.
[10] K. Lutchmiah, A.R.D. Verliefde, K. Roest, L.C. Rietveld, E.R. Cornelissen, Forward osmosis for application in wastewater treatment: a review, Water Res., 58 (2014) 179–197.
[11] T. Majeed, S. Phuntsho, S. Jeong, Y. Zhao, B. Gao, H.K. Shon, Understanding the risk of scaling and fouling in hollow fiber forward osmosis membrane application, Process Saf. Environ. Prot., 104 (2016) 452–464.
[12] A.D. Khawaji, Advances in seawater desalination technologies, Desalination, 221 (2008) 47–69.
[13] R. Semiat, Desalination: present and future, Water Int., 25 (2000) 54–65.
[14] P.G. Klepetsanis, P.G. Koutsoukos, Precipitation of calcium sulfate dihydrate at constant calcium activity, J. Cryst. Growth, 98 (1989) 480–486.
[15] D.H. Troup, J.A. Richardson, Scale nucleation on a heat transfer surface and its prevention, Chem. Eng. Commun., 2 (1978) 167–180.
[16] S.K. Hamdona, R.B. Nessim, S.M. Hamza, Spontaneous precipitation of calcium sulphate dihydrate in the presence of some metal ions, Desalination, 94 (1993) 69–80.
[17] S. Lee, J.-S. Choi, C.-H. Lee, Behaviors of dissolved organic matter in membrane desalination, Desalination, 238 (2009) 109–116.
[18] A. Antony, J.H. Low, S. Gray, A.E. Childress, P. Le-Clech, G. Leslie, Scale formation and control in high pressure membrane water treatment systems: a review, J. Membr. Sci., 383 (2011) 1–16.
[19] Q. She, R. Wang, A.G. Fane, C.Y. Tang, Membrane fouling in osmotically driven membrane processes: a review, J. Membr. Sci., 499 (2016) 201–233.
[20] T.Y. Cath, A.E. Childress, M. Elimelech, Forward osmosis: principles, applications, and recent developments, J. Membr. Sci., 281 (2006) 70–87.
[21] R.L. McGinnis, M. Elimelech, Energy requirements of ammonia–carbon dioxide forward osmosis desalination, Desalination, 207 (2007) 370–382.
[22] S.A. Avlonitis, M. Pappas, K. Moutesidis, A unified model for the detailed investigation of membrane modules and RO plants performance, Desalination, 203 (2007) 218–228.
[23] J. Gilron, D. Hasson, Calcium sulfate fouling of reverse osmosis membranes: flux decline mechanism, Chem. Eng. Sci., 42 (1987) 2351–2360.
[24] S. Lee, J. Kim, C.H. Lee, Analysis of $CaSO_4$ scale formation mechanism in various nanofiltration modules, J. Membr. Sci., 163 (1999) 63–74.
[25] S. Lee, C.H. Lee, Effect of operating conditions on $CaSO_4$ scale formation mechanism in nanofiltration for water softening, Water Res., 34 (2000) 3854–3866.
[26] S. Lee, R.M. Lueptow, Control of scale formation in reverse osmosis by membrane rotation, Desalination, 155 (2003) 131–139.
[27] B. Mi, M. Elimelech, Gypsum scaling and cleaning in forward osmosis: measurements and mechanisms, Environ. Sci. Technol., 44 (2010) 2022–2028.